

Charge transfer electrostatic model of compositional order in perovskite alloys.

Zhigang Wu and Henry Krakauer

Department of Physics, College of William and Mary

Williamsburg, VA 23187

(November 20, 2018)

Abstract

We introduce an electrostatic model including charge transfer, which is shown to account for the observed B-site ordering in Pb-based perovskite alloys. The model allows charge transfer between A-sites and is a generalization of Bellaiche and Vanderbilt's purely electrostatic model. The large covalency of Pb^{2+} compared to Ba^{2+} is modeled by an environment dependent effective A-site charge. Monte Carlo simulations of this model successfully reproduce the long range compositional order of both Pb-based and Ba-based complex $\text{A}(\text{BB}'\text{B}'')\text{O}_3$ perovskite alloys. The models are also extended to study systems with A-site and B-site doping, such as $(\text{Na}_{1/2}\text{La}_{1/2})(\text{Mg}_{1/3}\text{Nb}_{2/3})\text{O}_3$, $(\text{Ba}_{1-x}\text{La}_x)(\text{Mg}_{(1+x)/3}\text{Nb}_{(2-x)/3})\text{O}_3$ and $(\text{Pb}_{1-x}\text{La}_x)(\text{Mg}_{(1+x)/3}\text{Ta}_{(2-x)/3})\text{O}_3$. General trends are reproduced by purely electrostatic interactions, and charge transfer effects indicate that local structural relaxations can tip the balance between different B-site orderings in Pb based materials.

PACS numbers: 64.60.Cn, 81.30.-t, 77.84.-s, 77.84.Dy

I. INTRODUCTION

Complex solid solution perovskite structure based relaxor ferroelectrics such as $\text{Pb}(\text{Zr}_{1-x}\text{Ti}_x)\text{O}_3$ (PZT) and $(1-x)\text{Pb}(\text{Zn}_{1/3}\text{Nb}_{2/3})\text{O}_3 + x\text{PbTiO}_3$ (PZN-PT) show great promise as piezoelectric transducers. [1] In their simplest form, PZN-PT materials are B-site alloys of the form $\text{A}(\text{BB}'\text{B}'')\text{O}_3$, with three different B-site cations from group II, IV, and V, which exhibit compositionally dependent B-site atomic ordering. For example, at 1640 °C, when the tetravalent composition x is increased in $(1-x)\text{Ba}(\text{MgNb})\text{O}_3 + x\text{BaZrO}_3$ (BMN-BZ) alloy, the following sequence of B-site ordering is observed: $[111]_{1:2}$ order for $x < 5\%$; then $[111]_{1:1}$ order for $5\% < x < 25\%$; and finally disorder for larger x . [2] Other Ba-based perovskites, e.g., $(1-x)\text{Ba}(\text{Mg}_{1/3}\text{Ta}_{2/3})\text{O}_3 + x\text{BaZrO}_3$ (BMT-BZ), [2] $(1-x)\text{Ba}(\text{Mg}_{1/3}\text{Nb}_{2/3})\text{O}_3 + x\text{BaZrO}_3$ (BMN-BZ), [3] display a similar sequence of B-site order. On the other hand, for Pb-based systems, e.g., $(1-x)\text{Pb}(\text{Mg}_{1/3}\text{Ta}_{2/3})\text{O}_3 + x\text{PbZrO}_3$ (PMT-PZ), $[111]_{1:2}$ order is not observed at $x = 0$; instead, annealing between 1325°C and 1350°C results in $[111]_{1:1}$ order all the way down to $x = 0$. [4,5] Other Pb-based perovskites, e.g., $\text{Pb}(\text{Mg}_{1/3}\text{Nb}_{2/3})\text{O}_3$ (PMN), [6–8] display similar B-site ordering.

Chemical substitutions on the A-site can also strongly affect B-site ordering. For example, $(\text{Na}_{1/2}\text{La}_{1/2})(\text{Mg}_{1/3}\text{Nb}_{2/3})\text{O}_3$ shows $[111]_{1:1}$ B-site ordering at all measured temperatures; and $[001]_{1:1}$ A-site ordering occurs below $\sim 950^\circ\text{C}$. [9] In $(\text{Ba}_{1-x}\text{La}_x)(\text{Mg}_{(1+x)/3}\text{Nb}_{(2-x)/3})\text{O}_3$, $[111]_{1:1}$ B-site ordering is induced and coexists with $[111]_{1:2}$ order as low as 5% La doping on A-sites. For $x \geq 0.1$, $[111]_{1:1}$ B-site ordering is stabilized. [10] Similar B-site ordering sequences are observed for $(\text{Ba}_{1-x}\text{La}_x)(\text{Zn}_{(1+x)/3}\text{Nb}_{(2-x)/3})\text{O}_3$. [11] On the other hand, annealing $(\text{Pb}_{1-x}\text{La}_x)(\text{Mg}_{(1+x)/3}\text{Ta}_{(2-x)/3})\text{O}_3$ at 1300 °C yields $[111]_{1:1}$ B-site ordering for all x , and the strongest 1:1 reflections are measured at $x = 0.5$. [12] $(\text{Pb}_{1-x}\text{La}_x)(\text{Mg}_{(1+x)/3}\text{Nb}_{(2-x)/3})\text{O}_3$ displays similar B-site ordering sequence. [13]

Bellaiche and Vanderbilt (BV) introduced an electrostatic model that was remarkably successful in explaining the B-site ordering of $\text{A}^{+2}(\text{BB}')\text{O}_3$ perovskite alloys, using only electrostatic interactions between B-site. [14] However, the model failed to correctly describe the small x behavior of PMT-PZ described above. The BV model has also not been extended to study the effects of A-site chemical substitution.

The different behavior of Ba- and Pb-based alloys may be presumed to arise from the greater covalency of Pb compared to Ba. First-principles calculations for Ba based alloys show that typical B-site stacking structural energy differences can be as large as 60 kJ/(mol- ABO_3). [15] This is an order of magnitude larger than in similar Pb based alloys, [15–17] and reflects the greater covalency of Pb compared to Ba. In this paper, we investigate modeling Pb covalency through the inclusion of a local-configuration dependent A-site charge, *i.e.* charge transfer between A-sites. The resulting electrostatic models with and without charge transfer are used to study B-site atomic ordering in undoped and La-doped Ba- and Pb-based perovskite alloys.

II. ELECTROSTATIC MODELS WITHOUT CHARGE TRANSFER

We will be considering supercells of the ABO_3 perovskite structure with possible mixtures of different atomic species on the A and B sites. Strain and relaxation of atomic positions are neglected in all that follows. The total electrostatic energy is then given by

$$E = \frac{e^2}{2} \sum_{(l\tau) \neq (l'\tau')} \frac{Q_{l\tau} Q_{l'\tau'}}{\epsilon |\mathbf{R}_{l\tau} - \mathbf{R}_{l'\tau'}|}, \quad (1)$$

where l indexes the primitive cubic cell within the supercell, τ indicates the sublattice position in the l^{th} primitive cell ($\tau = \{A, B, O_1, O_2, O_3\}$), and ϵ is the electronic dielectric constant. The formal oxygen ionic charge $Q_{l,O} = -2$ will be used in the following, and the A- and B-site charges will be referenced to PbTiO_3 :

$$Q_{l,A} = 2 + \Delta q_{l,A}, \quad (2)$$

and

$$Q_{l,B} = 4 + \Delta q_{l,B}, \quad (3)$$

e.g. $\Delta q_{l,A} = 0, -1, +1$ for Ba, Na, and La respectively, and $\Delta q_{l,B} = 0, -2, +5$ for Ti, Mg, and Nb respectively, give the formal ionic charges for these atoms. BV showed that up to a constant, the configurationally averaged total energy depends only on terms quadratic in the $\Delta q_{l,\tau}$. The configurational electrostatic energy can then be written as:

$$E_{AB} = \frac{e^2}{2\epsilon} \left[\sum_{(lA) \neq (l'A')} \frac{\Delta q_{lA} \Delta q_{l'A'}}{|\mathbf{R}_{lA} - \mathbf{R}_{l'A'}|} + \sum_{(lB) \neq (l'B')} \frac{\Delta q_{lB} \Delta q_{l'B'}}{|\mathbf{R}_{lB} - \mathbf{R}_{l'B'}|} + 2 \sum_{lA, l'B} \frac{\Delta q_{lA} \Delta q_{l'B}}{|\mathbf{R}_{lA} - \mathbf{R}_{l'B}|} \right], \quad (4)$$

BV introduced this model for $A^{+2}(\text{BB}')\text{O}_3$ perovskite alloys. Since they only considered alloys for which A-sites are occupied by Ba or Pb, where $\Delta q_{l,A} = 0$, the configurational electrostatic energy then depends only on the B-sublattice:

$$E_B = \frac{e^2}{2\epsilon a} \sum_{l \neq l'} \frac{\Delta q_{l,B} \Delta q_{l',B}}{|l - l'|}, \quad (5)$$

where a is the cubic lattice constant, and $\mathbf{R}_l = l\mathbf{a}$.

This model was remarkably successful in explaining the B-site ordering of $A^{+2}(\text{BB}')\text{O}_3$ perovskite alloys using Eq. (5). [14] Using a B-site-only notation to describe the different classes of alloys simplifies the discussion. Thus, $\text{IV}_x \text{IV}'_{1-x}$ denotes a homovalent B-site binary alloy having tetravalent B-atoms, *e.g.*, $\text{Pb}(\text{ZrTi})\text{O}_3$; and $\text{II}_{(1-x)/3} \text{IV}_x \text{V}_{2(1-x)/3}$ indicates a heterovalent B-site ternary, such as $(1-x) \text{Ba}(\text{Mg}_{1/3} \text{Nb}_{2/3})\text{O}_3 + x \text{BaZrO}_3$. The BV model predicted the following B-site orderings [14]: (1) For $\text{III}_{(1-x)/2} \text{IV}_x \text{V}_{(1-x)/2}$ and $\text{II}_{(1-x)/2} \text{IV}_x \text{VI}_{(1-x)/2}$ heterovalent ternaries, a rocksalt-type $[111]_{1:1}$ ordering becomes disordered with progressively increasing x , consistent with experimental observations. (2) For $\text{II}_{(1-x)/3} \text{IV}_x \text{V}_{2(1-x)/3}$ heterovalent ternaries, the model predicts a richer phase diagram, with $[111]_{1:2}$ order for x less than about 5%, $[111]_{1:1}$ order for x greater than 5%, followed by disorder for large x . This is in good agreement with observations for Ba based systems but disagrees for Pb based systems, where $[111]_{1:1}$ order persists down to $x = 0$. They proposed a possible explanation, [14] postulating a small amount of Pb^{4+} on the B-sublattice to explain the stabilization of the 1:1 phase. As far as we know, there is no evidence of the presence of Pb^{4+} on the B-sublattice.

III. CHARGE TRANSFER ELECTROSTATIC MODEL

As mentioned, first-principles calculations for Ba based alloys show that typical B-site stacking structural energy differences can be as large as 60 kJ/(mol-ABO₃), [15] which is an order of magnitude larger than in the Pb based alloys. [15–17] The energy differences in the Ba based compounds can be approximately reproduced in the BV model by choosing the value of its one free parameter $\epsilon = 10$ at the experimental volume. [14,15] However, the BV model is then unable to account for the much smaller energy differences in the Pb based compounds. The greater covalency of Pb compared to Ba permits larger local relaxations, reducing the energy differences between different Pb based B-site stackings. Covalent interactions are of course absent in a purely electrostatic model.

We attempt to model the greater Pb covalency by allowing charge transfer between A-sites, depending on the local B-site configuration. Our charge transfer electrostatic model is closely patterned after similar models that were introduced to model the configuration dependence of Coulomb energies for pseudobinary alloys, [18–20] such as (Al_{0.5}Ga_{0.5})As. These calculations found that Coulomb contributions of calculated mixing enthalpies were commensurate with that of lattice mismatch energies. [18] In addition, the trend of stability of (AC)_n(BC)_n superlattices predicted by these models was consistent with first-principles total-energy calculations for lattice-matched semiconductor superlattices. [20]

To avoid confusion in the following, we use an overhead “ \sim ” to denote charges that depend on the local configuration of a site, while charges without the overhead \sim denote ionic charges that depend only on the atom occupying the site. The simplest way to include charge transfer in the model is to define a nearest-neighbor configuration-dependent effective A-site charge $\tilde{Q}_{l,A}$:

$$\tilde{Q}_{l,A} = q_A + \Delta\tilde{q}_{l,A} = 2 + \Delta\tilde{q}_{l,A} . \quad (6)$$

where

$$\Delta\tilde{q}_{l,A} = -\lambda \left(\frac{1}{8} \sum_{i=n.n.B\text{-sites}} \Delta q_{i,B} \right) . \quad (7)$$

The parameter λ controls the charge transfer between the A-sites, *i.e.* the degree of covalency on the A-site. Overall charge neutrality is automatically maintained by this expression. With this definition the configurationally dependent electrostatic energy now depends on both the A- and B-sublattices:

$$E_{AB} = \frac{e^2}{2\epsilon} \left[\sum_{(lA) \neq (l'A')} \frac{\Delta\tilde{q}_{lA} \Delta\tilde{q}_{l'A'}}{|\mathbf{R}_{lA} - \mathbf{R}_{l'A'}|} + \sum_{(lB) \neq (l'B')} \frac{\Delta q_{lB} \Delta q_{l'B'}}{|\mathbf{R}_{lB} - \mathbf{R}_{l'B'}|} + 2 \sum_{lA, l'B} \frac{\Delta\tilde{q}_{lA} \Delta q_{l'B}}{|\mathbf{R}_{lA} - \mathbf{R}_{l'B}|} \right] , \quad (8)$$

This expression is formally similar to Eq. (4), except that here the charge on an A-site depends not only on the atomic species on that site but on the nearest neighbor B-site configuration.

The value of the additional parameter λ can be chosen depending on the species occupying the A-site. Thus for Ba-based alloys $\lambda = 0$, no charge transfer occurs, and the model reduces to Bellaiche and Vanderbilt’s model. For Pb-based alloys, the value of λ can be fit to first-principles calculations of representative supercells of Pb(BB')O₃.

The parameters in our model are chosen as follows. ϵ is chosen to reproduce the energy differences of selected Ba-based alloys (we used $\epsilon = 10$, as in Ref. [15]). The value of λ is then fit to selected Pb-based alloy energy differences. Fig. 1 shows structural energy differences ($x = 0$) as a function of λ . To obtain B-site stacking structural energy differences in the range of 10 kJ/(mol- ABO_3) for Pb based alloys energies, as found in first-principles calculations, Fig. 1 indicates that λ_{Pb} should be chosen in the range $0.7 < \lambda_{\text{Pb}}$.

IV. MONTE CARLO SIMULATIONS

Metropolis Monte Carlo simulations [21] were carried out with periodic boundary conditions using $6 \times 6 \times 6$ supercells, similar to those in BV. To obtain good statistics, typically $\sim 10^7$ moves were made at each temperature. Calculations were started at at high temperature (e.g., 4000 K) with a random configuration, and the temperature was then slowly decreased until the acceptance rate becomes very low. To determine the B-site ordering the Fourier transform of the charge-charge correlation function $\eta(\mathbf{k})$ was computed from converged runs at a given temperature: [14]

$$\eta(\mathbf{k}) = \alpha \sum_{l'} \Delta q_l \Delta q_{l+l'} \exp(-i\mathbf{k} \cdot \mathbf{l}') , \quad (9)$$

where α is a normalization factor, the sum runs over the B-sublattice, and \mathbf{k} is the wavevector in the Brillouin zone of the unit cubic cell. The charge-charge correlation function $\eta(\mathbf{k})$ is directly proportional to the ensemble average of the square of the Fourier transform of the charge distribution, e.g., a large value of η at $\mathbf{k} = 2\pi(\frac{1}{2}, \frac{1}{2}, \frac{1}{2})$ or $\mathbf{k} = 2\pi(\frac{1}{3}, \frac{1}{3}, \frac{1}{3})$ corresponds to a strong $[111]_{1:1}$ or $[111]_{1:2}$ order respectively.

V. RESULTS

MC calculations using electrostatic models with and without charge transfer are reported in this section as a function of temperature and concentration x of A- and B-site doping. Results for B-site only alloys are presented first. A- and B-site alloy calculations are then considered, first using a purely electrostatic models and then including charge transfer.

A. B-site Alloys With Charge Transfer

Simulations were performed using Eqs. (7,8) for $\text{A}(\text{BB}'\text{B}'')\text{O}_3$ alloys with $\lambda = 0.3$ and 0.7 , and setting $a = 7.7$ a.u. and $\epsilon = 10$. Results for $\text{II}_{(1-x)/3}\text{IV}_x\text{V}_{2(1-x)/3}$ heterovalent ternaries are given in Fig. 2, which shows the calculated charge-charge correlation function $\eta(\mathbf{k})$ vs. tetravalent composition x at temperatures of $T = 1000$ K and 1500 K and for $\lambda = 0.3$ and 0.7 respectively. For $\lambda = 0.3$, which permits only a small charge transfer between A-sites, Bellaiche and Vanderbilt's prediction is reproduced (also for $\lambda = 0.0$, not shown), *i.e.* we obtain the B-site ordering sequence of Ba-based perovskite alloys described in Section II. For $\lambda = 0.7$, Fig. 2 shows there is no $[111]_{1:2}$ ordered phase. Instead, there is a continuous transformation from $[111]_{1:1}$ order at $x = 0$ to a disordered state at large x . Increasing the

final temperature to $T=1500\text{K}$ does not change this ordering sequence, but only decreases the value of x at which disorder appears, as expected.

Moreover, the $[111]_{1:1}$ structure is similar to the “random-site” model, [2] in that it has alternating planes of mixed (II-V)-planes and pure (V)-planes, as was also found by BV. These results are in good agreement with experimental observations of the ordering sequence of $\text{Pb}(\text{Mg}_{1/3}\text{Nb}_{2/3})\text{O}_3$ (PMN), [6–8] $(1-x)\text{Pb}(\text{Mg}_{1/3}\text{Ta}_{2/3})\text{O}_3 + x\text{PbZrO}_3$ (PMT-PZ) [4] and $\text{Pb}(\text{Mg}_{1/3}\text{Ta}_{2/3})\text{O}_3$ (PMT). [5]

The charge transfer model also correctly predicts B-site ordering in the $\text{III}_{(1-x)/2}\text{IV}_x\text{V}_{(1-x)/2}$ and $\text{II}_{(1-x)/2}\text{IV}_x\text{VI}_{(1-x)/2}$ alloys. Monte Carlo simulations using Eqs. (7,8) with $\lambda = 0$ and $\lambda = 0.7$ show that both Ba-based and Pb-based perovskite alloys have the same B-site ordering for $\text{III}_{(1-x)/2}\text{IV}_x\text{V}_{(1-x)/2}$ ternaries and $\text{II}_{(1-x)/2}\text{IV}_x\text{VI}_{(1-x)/2}$ ternaries. Our results reproduce those of BV in these cases.

B. A- and B-site Alloys Without Charge Transfer

To study the effects of A-site chemical substitution, we first used a purely electrostatic model with formal ionic charges. Calculations were performed for $(\text{A}_{1/2}^{1+}\text{A}'_{1/2}{}^{3+})(\text{B}_{1/3}^{2+}\text{B}'_{2/3}{}^{5+})\text{O}_3$ and $(\text{A}_{1-x}^{2+}\text{A}'_x{}^{3+})(\text{B}_{(1+x)/3}^{2+}\text{B}'_{(2-x)/3}{}^{5+})\text{O}_3$. Since $Q_{l,A}$ is now not a constant, we express the A- and B-sublattice charges using Eq. (4).

Fig. 3 shows both A- and B-site charge-charge correlation function $\eta(\mathbf{k})$ vs. temperature for $(\text{A}_{1/2}^{1+}\text{A}'_{1/2}{}^{3+})(\text{B}_{1/3}^{2+}\text{B}'_{2/3}{}^{5+})\text{O}_3$. The purely electrostatic model, Eq. (4), can explain the observed $[111]_{1:1}$ B-site ordering of $(\text{Na}_{1/2}\text{La}_{1/2})(\text{Mg}_{1/3}\text{Nb}_{2/3})\text{O}_3$. [9] Moreover, the 1:1 B-site ordering found in the calculations corresponds to the random site model. As seen in Fig. 3, weak $[001]_{1:1}$ A-site ordering is also obtained in the simulations, in agreement with measurements on samples annealed below $\sim 950^\circ\text{C}$ [9]. Perfect $[001]_{1:1}$ A-site ordering would correspond to alternating $[001]$ A-planes of Na and La, but the A-sites in the simulations are more disordered (see section VI). In simulations using a $6\times 6\times 6$ supercell, only B-site order was observed. The weak A-site ordering emerged only after increasing the simulation region to a larger $12\times 12\times 12$ supercell.

Fig. 4 shows $\eta(\mathbf{k})$ vs. tetravalent composition x for $(\text{A}_{1-x}^{2+}\text{A}'_x{}^{3+})(\text{B}_{(1+x)/3}^{2+}\text{B}'_{(2-x)/3}{}^{5+})\text{O}_3$. The symmetry about $x = 0.5$ is a consequence of our model. Exchanging x with $1-x$ in Eq. (4), every $\Delta q_{l\tau}$ changes sign, and the configurational energy is unchanged. The strongest $[111]_{1:1}$ B-site order occurs at $x = 0.5$, in agreement with experiment. Experimentally, $(\text{Ba}_{1-x}\text{La}_x)(\text{Zn}_{(1+x)/3}\text{Nb}_{(2-x)/3})\text{O}_3$ (BLZN) exhibits 1:2 ordering coexisting with 1:1 B-site order for x less than ~ 0.05 , then switching to 1:1 B-site order for $0.05 < x < 0.6$. [11] $(\text{Ba}_{1-x}\text{La}_x)(\text{Mg}_{(1+x)/3}\text{Nb}_{(2-x)/3})\text{O}_3$ (BLMN) behaves similarly except that 1:1 B-site order is observed over the whole range $0.05 < x < 1$. [10] Fig. 4 shows that the purely electrostatic model, Eq. (4), correctly reproduces the observed B-site ordering, except for the extreme La-rich $x > 0.95$ region, where Eq. (4) incorrectly predicts 1:2 ordering. However, including charge transfer (see below) improves the agreement with experiment in the extreme La-rich region (section C below).

The character of the 1:1 B-site order in Fig. 4 changes at $x = 1/2$. A detailed examination of the equilibrated Monte Carlo structures shows that the 1:1 order results from a $[111]$ rocksalt-like alternation of β' and β'' layers. For $x < 0.5$ we find

$[\beta']_{1/2}[\beta'']_{1/2} = [(B_{(2+2x)/3}^{2+})(B_{(1-2x)/3}^{5+})]_{1/2}[B^{5+}]_{1/2}$, *i.e.* the β' site is a mixture of B^{+2} and B^{+5} atoms, and the β'' site is solely occupied by B^{+5} atoms. This is consistent with the “random-site” model. The peak in the 1:1 order parameter at $x = 0.5$ in Fig. 4 corresponds to $[\beta']_{1/2} = [B^{2+}]_{1/2}$, so the β' and β'' are each occupied by a single cation species, and the 1:1 reflections [10] exhibit their maximum intensity. However, for $0.5 < x$ we find $[\beta']_{1/2}[\beta'']_{1/2} = [B^{2+}]_{1/2}[(B_{(2x-1)/3}^{2+})(B_{(4-2x)/3}^{5+})]_{1/2}$, where now the β' site is solely occupied by B^{+2} atoms and the β'' site is now a mixture of B^{+2} and B^{+5} atoms. Akbas et al. [11,10,12] proposed this structure based on their observations.

C. A- and B-site Alloys With Charge Transfer

We next consider whether the inclusion of charge transfer may improve the agreement with experiment for the A- and B-site alloys considered in the previous section. The electronegativity and electron affinity of an atom is an indicator of the degree of covalency. By this measure, La is more covalent than Ba or Na, and Nb has higher covalency than Ta.

There is a difficulty in generalizing our charge transfer model to systems with more than one atomic species on the A- and B-sites, such as $(Ba_{1-x}La_x)(Mg_{(1+x)/3}Nb_{(2-x)/3})O_3$. Considering charge transfer only onto La ions and using Eq. (7), charge neutrality may be violated except for $x = 1$. For BLMN, the simplest way to restore charge neutrality is to permit charge transfer onto both La and Ba ions, using an average charge transfer parameter $\lambda_A(x)$ proportional to the La composition x , *i.e.*, $\lambda_A(x) = x\lambda_A(1)$, so that there is no charge transfer at $x = 0$ (BMN) and the largest charge transfer occurs for at $x = 1$ (LMN).

In BLMN alloys, charge transfer onto B-sites may also be considered. Mg is pure ionic, but Nb and Ta are more polarizable. To ensure charge neutrality we may define λ_B similar to λ_A :

$$\lambda_B(x) = \frac{(2-x)}{3}\lambda_A(1), \quad (10)$$

which varies linearly with B^{+5} concentration. The configurationally dependent charges on the A-sites and B-sites are then defined as:

$$\Delta\tilde{q}_{l,A} = -\lambda_A(x)\left(\frac{1}{8}\sum_{i=n.n.B\text{-sites}}\Delta q_{i,B}\right), \quad (11)$$

$$\Delta\tilde{q}_{l,B} = -\lambda_B(x)\left(\frac{1}{8}\sum_{i=n.n.A\text{-sites}}\Delta q_{i,A}\right), \quad (12)$$

where

$$\Delta q_{l,\tau} = Q_{l,\tau} - q_\tau, \quad (13)$$

where, $\tau = \{A,B\}$, $Q_{l,\tau}$ is the formal charge, and q_A and q_B are the mean charge of A-sites and B-sites respectively.

We first consider BLMN. To test this model, we set $\lambda_A(1) = 0.7$, since LMN is observed to have $[111]_{1:1}$ B-site ordering. Fig. 5 shows $\eta(\mathbf{k})$ as a function of La composition x for

BLMN. The main effect of including charge transfer is that 1:1 order now appears in the La-rich region. There is essentially no difference in the B-site ordering with and without charge transfer onto the B-sites. Both display $[111]_{1:2}$ order at small x ($x < 3\%$), then $[111]_{1:2}$ and $[111]_{1:1}$ order coexist at $3\% < x < 5\%$, and finally $[111]_{1:1}$ order for all $x > 5\%$. However, the model introduces features not seen in the measurements of BLMN. [10] The peak of $[111]_{1:1}$ order shifts from $x = 0.5$ to $x \sim 0.35$, and there is a dip in $\eta(\mathbf{k})$ for $[111]_{1:1}$ order at $x \sim 0.8$.

The replacement of Ba by Pb in the La-doped perovskites ($\text{Pb}_{1-x}\text{La}_x$) ($\text{B}_{(1+x)/3}^{2+}\text{B}'_{(2-x)/3}^{5+}$) O_3 is now considered. For PLMN, 1:1 B-site ordering is observed for La concentrations, increasing continuously up to $x = 0.5$ and the decreasing for $x > 0.5$. Again, this trend is consistent with Fig. 4, except that the purely electrostatic model results in 1:2 order in the extreme Pb and La rich regions. [12] Several choices for the charge transfer parameter were considered. Assuming first that La is much less covalent than Pb, the charge transfer constant is chosen to be proportional to the Pb concentration, $\lambda_A(x) = (1-x)\lambda_A(1)$, so that there is no charge transfer at $x = 1$ (LMN) and the largest charge transfer occurs for at $x = 0$ (PMN). The resulting B-site ordering would be similar to Fig. 5, but with x mapped to $1-x$. Compared to Fig. 4, this improves the agreement with experiment for the Pb-rich alloys, yielding 1:1 B-site order. However, for La concentrations greater than about 95% the model does not yield the observed 1:1 ordering. [12] On the other hand assuming that La and Pb are similarly covalent, λ_A is set to a constant, $\lambda_A = 0.7$ as in PMN. The results are shown in Fig. 6. This model agrees with experiment in the Pb-rich and La-rich regions, reproducing the observed 1:1 B-site ordering, but is disordered for intermediate concentrations. Including charge transfer onto the B-sites with $\lambda_B(x) = 0.7\frac{(2-x)}{3}$ (not shown) yields similar results to those with charge transfer on A-sites only.

VI. DISCUSSION

First-principles calculations show that the energy differences between different B-site stackings of Pb-based [15–17] alloys are greatly reduced compared to those of Ba-based [15] alloys. For example, the energy differences between $[100]_{1:2}$, $[110]_{1:2}$, $[111]_{1:2}$ B-site stackings are reduced from ~ 60 kJ/(mol- ABO_3) in Ba-based alloys to ~ 5 kJ/(mol- ABO_3) in Pb-based alloys. [15] The energy reduction can be attributed to the greater covalency of Pb compared to Ba, which results in larger local relaxation energies in Pb-based compared to Ba-based alloys. As shown in Fig. 1, there is a dramatic decrease in structural energy differences when charge transfer between A-sites is included.

The magnitude of local relaxation energies due to Pb's greater covalency but *not including* charge transfer between A-sites can be estimated as follows. The ferroelectric PbTiO_3 double-well has a depth of ~ 10 kJ/(mol- ABO_3) not including strain, which is much larger than the well depth in BaTiO_3 , consistent with the more covalent nature of Pb. [22] However 10 kJ/(mol- ABO_3) is still not enough to account for the reduction from the 60 kJ/(mol- ABO_3) B-site stacking energy differences in Ba-based alloys. In heterovalent B-site alloys, however, charge transfer between A-sites is another possible local relaxation mechanism.

This is especially true for small x in B-site ternaries like $\text{II}_{(1-x)/3}\text{IV}_x\text{V}_{2(1-x)/3}$. Since the A-site has a nearest neighbor shell of eight B-sites, each of which is occupied by a $\Delta q_{l,B} = -2$ or $\Delta q_{l,B} = +1$ ion (for $x = 0$), the sum of these eight $\Delta q_{l,B}$ will necessarily be non-zero in

the $x = 0$ limit. By contrast, in $\text{III}_{(1-x)/2}\text{IV}_x\text{V}_{(1-x)/2}$ and $\text{II}_{(1-x)/2}\text{IV}_x\text{VI}_{(1-x)/2}$ alloys this “non-neutrality” condition is not forced. Our model simulates the effective charge transfer between A-sites that results from a combination of oxygen and Pb atomic relaxations and direct electronic charge transfer. The purely ionic character of Ba inhibits this, but the greater covalency of Pb makes this an effective mechanism to increase the local relaxation energy.

Local relaxation in Pb based alloys plays an important role in compensating the purely electrostatic energy differences arising from different B-site stackings. The electrostatic charge transfer model in Section III correctly describes the observed B-site ordering in PMN type B-site $\text{II}_{(1-x)/3}\text{IV}_x\text{V}_{2(1-x)/3}$ heterovalent ternaries. As shown by Fig. 2, introducing charge transfer changes the small x ordering from $[111]1:2$ to the $[111]1:1$ ordering seen experimentally.

While improving agreement with experiment for II-IV-V B-site alloys, the inclusion of charge transfer does not alter the correct B-site ordering predictions of the BV model for the III-IV-V and II-IV-VI alloys. For these alloys, the simulations predict a rocksalt-like structure where the A-site has on average a “neutral” nearest neighbor shell of B-sites. In this case, the average $\Delta\tilde{q}_A$ will be small for any value of λ . Direct Monte Carlo calculations using our charge transfer model predict the same B-site ordering as the purely electrostatic model of Bellaiche and Vanderbilt.

A detailed analysis of our results supports the random-site model of the $[111]1:1$ ordered regions. We do not find any evidence for the space-charge model. In the space-charge model, as discussed in Ref. [2], the 1:1 ordered regions correspond to a rock-salt like $[111]$ stacking of alternating II:V planes, which is locally charge-imbalanced. In the space-charge scenario, Coulomb repulsion would limit the size of these charge-imbalanced regions to nanoscale size. Overall charge neutrality is restored by embedding the nanoscale 1:1 regions in a disordered (+5 ion)-rich matrix. The space-charge model was long favored, because it could explain the failure of high temperature annealing to increase the size of these 1:1 regions. Instead, the recent successful coarsening of these 1:1 regions [2] would seem to rule out charge-imbalanced 1:1 regions. The random-site model is also supported by recent direct Z-contrast imaging in PMN. [23]

Indeed, our calculations show that the $[111]1:1$ ordering corresponds to alternating (II-V):V planes, *i.e.* planes with a random mixture of (II-V) cations alternating with pure V planes. Bellaiche and Vanderbilt also observed this structure in their 1:1 ordered regions. This stacking is consistent with the random-site model. In materials that are also A-site alloys, our calculations reveal interesting variants of the random-site model, as discussed below.

The results of A- and B-site alloy B-site ordering presented in the previous section show that the purely electrostatic model, Eq. (4), can account for many of the observations. For $(\text{Na}_{1/2}\text{La}_{1/2})(\text{Mg}_{1/3}\text{Nb}_{2/3})\text{O}_3$ Dupont *et al.* [9] argued that $[111]1:2$ B-site order is incompatible with the different valences of the A-site cations. In the $[111]1:2$ structure there are two types of environments for the A-site. In the first, two A-sites are located between a B^{5+} and a B^{2+} layer and have 5 B^{5+} and 3 B^{2+} nearest neighbors. The formal charge on these subcells is $[(5(+5) + 3(+2))/8 - 6] = -2.125$. The second A-site is located between two B^{5+} layers and has 6 B^{5+} and 2 B^{2+} nearest neighbors, with a subcell formal charge of -1.75. With a 1:1 mixture of Na^{+1} and La^{+3} on the A-sites, each cation must occupy both

types of A-site, leading to local charge imbalances of -1.125 and -0.75 for Na and +0.875 and +1.25 for La on the two respective type of A-sites. These are much larger than the charge imbalances when all A-site are occupied by divalent cations, namely -0.125 and +0.25, respectively. By contrast, in the random-site 1:1 B-site order structure, all the A-sites are equivalent and have 4 B^{5+} and 4 ($B_{2/3}^{5+}$ $B_{1/3}^{5+}$) neighbors, with a formal subcell charge of -2. This leads to local charge imbalances of -1 for Na and +1 for La. Dupont *et al.* noted that this reduction could be a factor in promoting the [111]1:1 B-site ordered structure. The MC results in Fig. 3, using the electrostatic-only model, confirm that 1:1 order can arise from purely electrostatic interactions.

As mentioned, the weak A-site ordering was not seen in simulations using a $6 \times 6 \times 6$ supercell, but only in the larger $12 \times 12 \times 12$ supercell shown. The large error bars in Fig. 3 reflect the difficulty in equilibrating this system at the lower temperatures in the Monte Carlo runs. This is probably due to the presence of many structural states with nearly degenerate energies. Perfect $[001]_{1:1}$ A-site ordering would correspond to alternating $[001]$ A-planes of Na and La, but this is not seen in the simulations and is reflected in the small value of the order parameter. To test if perfect $[001]_{1:1}$ A-site ordering is a global energetic minimum, we constrained the A-sites to have this ordering and allowed only the B-site configuration to change. This resulted in much weaker $[111]_{1:1}$ B-site order than seen in Fig. 3 and indicates the complex nature of the A-site order.

In BLMN, Fig. 4 shows that purely electrostatic interactions alone can account for stabilization of 1:2 B-site ordering for small La concentrations, switching to 1:1 ordering for larger concentrations. The experimentally observed 1:1 reflections [10] also have a peak at $x = 0.5$, which is consistent with the random-site model. For $x < 0.5$ we find the β' site is occupied by a random mixture of B^{+2} and B^{+5} atoms, while for $x > 0.5$ the β'' site is occupied by a random mixture. At $x = 0.5$, the β' and β'' are each occupied by a single cation species, yielding a peak in the 1:1 reflections. Experimentally, the 1:1 ordering persists up to the extreme La rich region [10]. However, the intensity of the 1:1 ordering reflections decreases between $0.5 < x < 1.0$, as reproduced by Fig. 4. Akbas and Davies have argued that the 1:2 structure structure is stabilized by anion displacements. In BMN, 1:2 MNN ordering into separate B^{+2} and B^{+5} layers permits adjacent anion layers to undergo a concerted displacement towards the smaller B^{+5} ion. This requires Nb cations to have an asymmetric anion coordination. For $x = 1$ (LMN), 1:2 MMN ordering would lead to an asymmetric environment for Mg, which is rarely observed. [10] Akbas and Davies argued that this stabilizes the 1:1 ordered phase for $x = 1$. The present calculations show that purely electrostatic interactions alone stabilize the 1:2 ordering near $x = 0$ and $x = 1$, since atomic displacements are not included. The results in Fig. 5 and 6 show that 1:1 order at $x = 1$ can be stabilized by the inclusion of charge transfer, which serves to reduce the energy differences between different B-site orderings, as shown in Fig. 1. For BLMN and PLMN, we interpret this charge transfer as modeling larger local structural relaxations for La than for Ba, tipping the balance slightly in favor of 1:1 ordering.

VII. CONCLUSIONS

We have used electrostatic models with and without charge transfer to study B-site ordering in materials with alloying on both the A- and B-sites. For Pb^{2+} and possibly other

covalent ions, the effective charge on the A-site can depend on the local B-site configuration. The inclusion of charge transfer into the electrostatic model of Bellaiche and Vanderbilt is shown to reproduce the observed B-site ordering in PMN type ternary perovskite alloys. For A- and B-site alloys, general trends are reproduced by purely electrostatic interactions. In $(\text{Na}_{1/2}\text{La}_{1/2})(\text{Mg}_{1/3}\text{Nb}_{2/3})\text{O}_3$, electrostatic effects alone produce B-site and A-site ordering observed in experiments. Charge transfer effects in simulations for Pb-based A- and B-site alloys indicate that local structural relaxations can tip the balance between different B-site orderings in some cases. With the inclusion of charge transfer in these cases, we conclude that the electrostatic interaction is the leading mechanism responsible for the B-site ordering in perovskite alloys.

ACKNOWLEDGMENTS

This work is supported by the Office of Naval Research grant N00014-97-1-0047. We acknowledge useful discussions with Peter Davies and Shiwei Zhang. We are grateful to Suhuai Wei for discussions on electrostatic models incorporating charge transfer.

REFERENCES

- [1] K. Uchino, *Piezoelectric Actuators and Ultrasonic Motors (Electronic Materials–Science & Technology, 1)*, (Kluwer Academic Publishers, Boston, 1996).
- [2] M.A. Akbas and P.K. Davies, *Solid State Chemistry of Inorganic Materials*, ed. P.K. Davies, A.J. Jacobson, C.C. Torardi, T and Vanderah, *Proceedings* **453**, 483 (1997).
- [3] L. Chai, M.A. Akbas, P.K. Davies, and J.B. Parise, *Materials Research Bulletin Pergamon* **32** (1997).
- [4] M.A. Akbas and P.K. Davies, submitted as a Communication to *J. Am. Ceram. Soc.* (may, 1997).
- [5] M.A. Akbas and P.K. Davies, *Journal of Materials Research*. **12**, 2617 (1997).
- [6] E. Husson, *Mat. Res. Bull.* **25**, 539 (1990).
- [7] E. Husson, *Mat. Res. Bull.* **23**, 357 (1988).
- [8] J. Chen, *J. Am. Cer. Soc.* **72**, 593 (1989).
- [9] L. Dupont, L. Chai, P.K. Davis, *Proceedings Materials Research Society, Solid State Chemistry of Inorganic Materials II*, **547**, 93-98 (1999).
- [10] M.A. Akbas and P.K. Davies, *J. Am. Ceram. Soc.* **81**, 2205 (1998).
- [11] M.A. Akbas and P.K. Davies, *J. Am. Ceram. Soc.* **81**, 1061 (1998).
- [12] J.K. Montgomery, M.A. Akbas and P.K. Davies, *J. Am. Ceram. Soc.* **82**, 3481 (1999).
- [13] M.A. Akbas and P.K. Davies, *J. Am. Ceram. Soc.* **83**, 119 (2000).
- [14] L. Bellaiche and D. Vanderbilt, *Phys. Rev. Lett.* **81**, 1318 (1998).
- [15] B. Burton and E. Cockayne, *Phys. Rev. B* **60**, 12542 (1999).
- [16] M. Wensell and H. Krakauer, AIP Proceedings.
- [17] M. Wensell and H. Krakauer, to be published.
- [18] M. van Schilfgaarde, A.-B. Chen, and A. Sher, *Phys. Rev. Lett.* **57**, 1149 (1986).
- [19] S.-H. Wei, *Phys. Rev. Lett.* **59**, 2613 (1987).
- [20] R. Magri, S.-H. Wei, A. Zunger, *Phys. Rev. B* **42**, 11388 (1990).
- [21] N. Metropolis *et al.*, *J. Chem. Phys.* **21**, 1087 (1953).
- [22] R. E. Cohen and H. Krakauer, *Ferroelectrics* **136**, 65 (1992).
- [23] Z. Xu, S. M. Gupta, and D. Viehland, *J. Am. Ceram. Soc.* **83**, 181 (2000).

FIGURES

Fig. 1 Wu and Krakauer

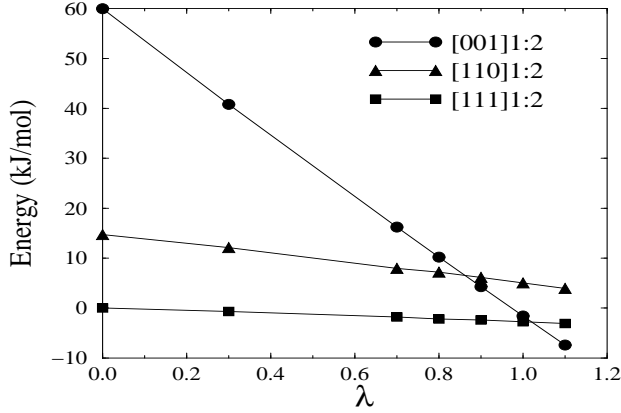


FIG. 1. Total energies (per mol = ABO_3) for 15-atom supercell 1:2 B-site stackings of $\text{A}(\text{B}_{1/3}\text{B}'_{2/3})\text{O}_3$. Energies are relative to the $\lambda = 0$ value of $[\text{111}]_{1:2}$.

Fig. 2 Wu and Krakauer

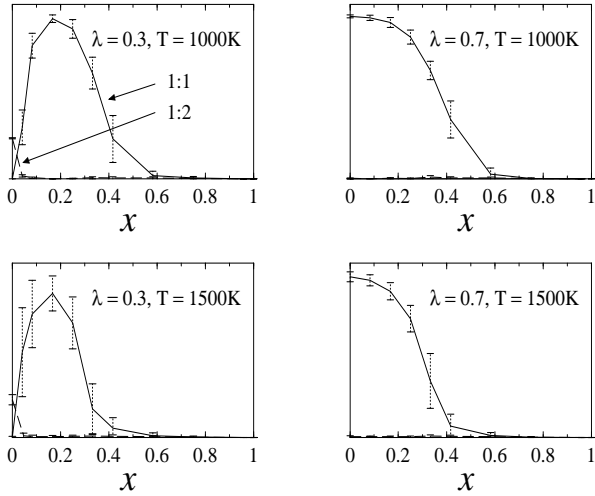


FIG. 2. Monte Carlo simulations of the long-range order parameter $\eta(\mathbf{k})$ vs. tetraivalent atomic composition x using the charge transfer model for $\text{II}_{(1-x)/3}\text{IV}_x\text{V}_{2(1-x)/3}$ ternaries, with $6 \times 6 \times 6$ supercells, $a = 7.7$ a.u., and $\epsilon = 10$.

Fig. 3 Wu and Krakauer
12x12x12 supercell

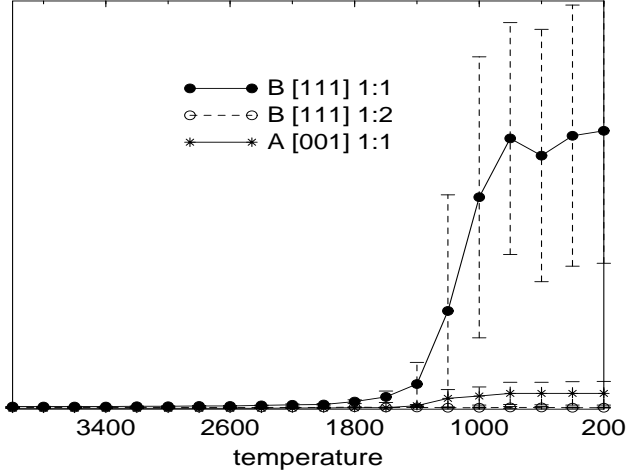


FIG. 3. Monte Carlo simulations of the long-range order parameters $\eta(\mathbf{k})$ vs. temperature T using BV model for $(A_{1/2}^{1+}A_{1/2}'^{3+})(B_{1/3}^{2+}B_{2/3}'^{5+})O_3$ perovskites, with $12 \times 12 \times 12$ supercells, $a = 7.5$ a.u., and $\epsilon = 10$.

Fig. 4 Wu and Krakauer

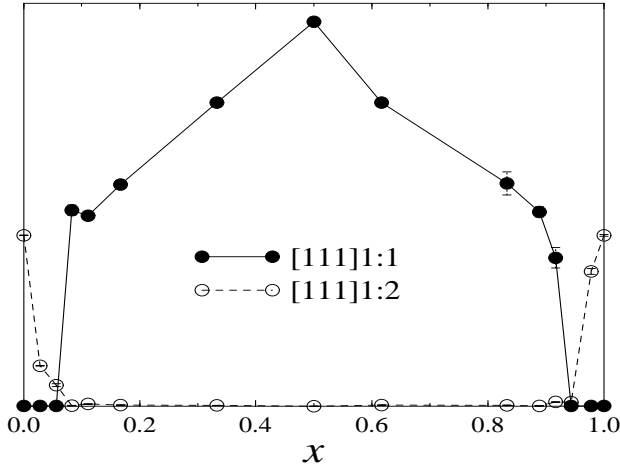


FIG. 4. Monte Carlo simulations of the long-range order parameter $\eta(\mathbf{k})$ vs. $A_x'^{3+}$ composition x using BV model for $(A_{1-x}^{2+}A_x'^{3+})(B_{(1+x)/3}^{2+}B_{(2-x)/3}'^{5+})O_3$ perovskites, with $6 \times 6 \times 6$ supercells, $a = 7.5$ a.u., and $\epsilon = 10$, at temperature $T = 1000$ K.

Fig. 5 Wu and Krakauer

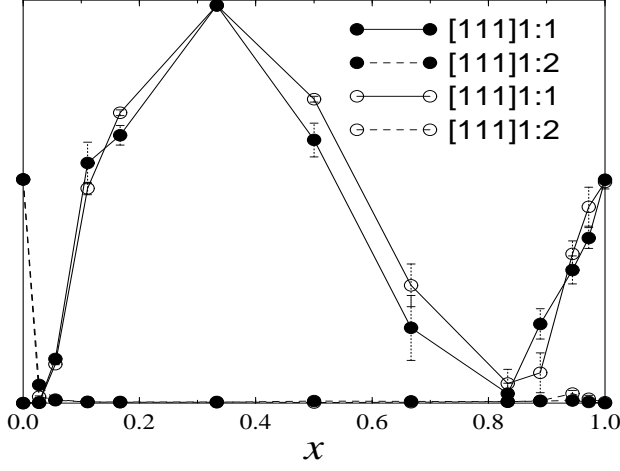


FIG. 5. Monte Carlo simulations of the long-range order parameter $\eta(\mathbf{k})$ vs. La composition x using charge transfer model for $(\text{Ba}_{1-x}\text{La}_x)(\text{B}_{(1+x)/3}^{2+}\text{B}'_{(2-x)/3}{}^{5+})\text{O}_3$ perovskites, with $6 \times 6 \times 6$ supercells, $a = 7.5$ a.u., and $\epsilon = 10$, at temperature $T = 1000$ K, $\lambda_A(x) = 0.7x$, $\lambda_B(x) = 0.7(2-x)/3$. The solid symbols denote charge transfer only on A-sites, and the unfilled symbols denote charge transfer on both A-sites and B-sites.

Fig. 6 Wu and Krakauer

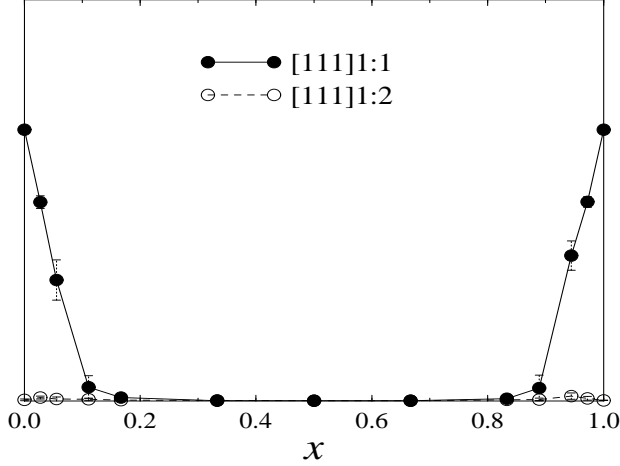


FIG. 6. Monte Carlo simulations of the long-range order parameter $\eta(\mathbf{k})$ vs. La composition x using charge transfer model only on A-sites for $(\text{Pb}_{1-x}\text{La}_x)(\text{B}_{(1+x)/3}^{2+}\text{B}'_{(2-x)/3}{}^{5+})\text{O}_3$ perovskites, with $6 \times 6 \times 6$ supercells, $a = 7.5$ a.u., and $\epsilon = 10$, at temperature $T = 1000$ K. $\lambda_A = 0.7$.